3D PRINTING

A silicone-based support material eliminates interfacial instabilities in 3D silicone printing

Senthilkumar Duraivel[1], Dimitri Laurent[2], Didier A. Rajon[2], Georg M. Scheutz[3], Abhishek M. Shetty[4], Brent S. Sumerlin[3], Scott A. Banks[5], Frank J. Bova[2], Thomas E. Angelini[1,5,6]*

Among the diverse areas of 3D printing, high-quality silicone printing is one of the least available and most restrictive. However, silicone-based components are integral to numerous advanced technologies and everyday consumer products. We developed a silicone 3D printing technique that produces precise, accurate, strong, and functional structures made from several commercially available silicone formulations. To achieve this level of performance, we developed a support material made from a silicone oil emulsion. This material exhibits negligible interfacial tension against silicone-based inks, eliminating the disruptive forces that often drive printed silicone features to deform and break apart. The versatility of this approach enables the use of established silicone formulations in fabricating complex structures and features as small as 8 micrometers in diameter.

Silicone elastomer's resistance to heat, chemical agents, weathering, ozone, moisture, and ultraviolet (UV) irradiation makes it critical for manufacturing countless products, including electronic devices, automobiles, aircraft, and medical devices (*1*). Silicone elastomers have been used in medical devices for many years (*2*), and their applications include embedded sensors (*3*), flexible electronics (*4*), soft robotics (*5*), and additive manufacturing (*6*). Silicone structures can be fabricated by using conventional techniques such as molding, or advanced techniques such as soft lithography and 3D printing (*7*–*9*). However, 3D printing with silicone generally results in low-quality products because of challenges created by the interfacial behaviors of silicone pre-elastomer in its liquid state. These challenges can be partially addressed by using an embedding support material that flows around the translating printing nozzles while trapping deposited inks in space, providing stability to printed structures (*10*–*14*). However, even under such stabilizing conditions, the interfacial tension between printed inks and their support media drives the deformation and breakup of printed structures before they solidify (Fig. 1, A and B) (*9*, *15*). Modifying silicone inks with additives can stabilize 3D printed structures (*16*, *17*), yet a versatile approach to additive manufacturing with unmodified silicone inks remains elusive. One route to achieving high-quality 3D silicone printing without ink modification is to eliminate the disruptive role of interfacial tension by using support materials that are chemically similar to the printed inks they stabilize (Fig. 1C). Thus, there is a critical need to develop support materials that are chemically similar to poly(dimethylsiloxane) (PDMS) inks.

We describe a method for 3D printing precise, intricately detailed structures made from PDMS that makes use of a support material exhibiting negligible interfacial tension when in contact with silicone inks. We call this method additive manufacturing at ultralow interfacial tension (AMULIT). The AMULIT support material is a packed inverse emulsion composed of aqueous droplets in a continuum of silicone oil. The ultralow interfacial tension between the AMULIT support material and PDMS inks enabled us to print features with diameters as small as 8 μm. We achieved high-performance printing by tuning the elasticity and flow properties of this support material, which allowed us to fabricate complicated shapes such as brain aneurysm models and functional trileaflet heart valves. We demonstrated that the AMULIT technique does not require specialized inks by using several different commercially available PDMS formulations to print various structures. With mechanical testing, we found that 3D printed structures produced by using AMULIT were more extensible than their molded counterparts and equally robust. We also found that these structures have a smooth surface finish at the macroscale and microscale roughness, which is facilitated by the low interfacial tension between PDMS inks and the AMULIT support medium. Our results show that the AMULIT 3D printing technique could be used to fabricate intricate silicone structures for biomaterial design and surgical simulators, and they introduce the possibility of expanding the method for printing with other materials.

[1]Department of Materials Science and Engineering, University of Florida, Gainesville, FL 32603, USA. [2]Department of Neurosurgery, University of Florida College of Medicine, Gainesville, FL 32608, USA. [3]George and Josephine Butler Polymer Research Laboratory, Center for Macromolecular Science and Engineering, Department of Chemistry, University of Florida, Gainesville, FL 32611, USA. [4]Advanced Technical Center, Anton Paar USA, Ashland, VA 23005, USA. [5]Department of Mechanical and Aerospace Engineering, University of Florida, Gainesville, FL 32611, USA. [6]J. Crayton Pruitt Family Department of Biomedical Engineering, University of Florida, Gainesville, FL 32611, USA.
*Corresponding author. Email: t.e.angelini@ufl.edu

Results

Formulation and testing of AMULIT support material

To formulate an AMULIT support medium for 3D printing with PDMS inks, we prepared inverse emulsions in which silicone oil was the continuous phase and varied the aqueous droplet packing fraction, ϕ, and the average droplet radius, a, between samples; ϕ and a can be tuned independently to determine an emulsion's rheological properties and its corresponding performance as a printing support medium (*18*). We expected a to strongly influence the printed feature roughness because the material interfaces will not spontaneously flatten under conditions of ultralow interfacial tension. Thus, we formulated small emulsion droplets and chose ϕ on the basis of the emulsions' rheological properties (fig. S1). The elastic shear modulus, G', and yield stress, σ_y, of each formulation, were measured with rheological tests (materials and methods and fig. S2). For AMULIT printing, we chose an emulsion having σ_y = 9 Pa and G' = 320 Pa; the emulsion with these properties is weak enough to flow around a translating printing needle yet strong enough to support complex 3D printed structures (*9*, *10*). For this formulation, we estimated the Reynolds number near the translating nozzle during a typical print to be 10^{-6} to 10^{-2}, which indicates that irregular flow patterns should be suppressed (supplementary text). For all formulations, we found that emulsions made from pure water droplets in silicone oil were extremely cloudy and inhibited visualizing the printing process. To make optically clear emulsions, we matched the refractive indices of the two phases by adding glycerol to the droplets, which allowed the 3D printing process to be imaged at the macroscale with photography and at the microscale with confocal fluorescence microscopy (CFM) (Fig. 1, D to G, and fig S3).

To test the role of interfacial tension in embedded 3D printing, we compared the performance of the AMULIT support medium with an all-aqueous support medium made from packed hydrogel microparticles swollen in water. In both cases, we 3D printed features made from a fluorescent PDMS liquid and imaged the ink-support interfaces using CFM (materials and methods). We formulated the packed microgels to have σ_y = 10 Pa and G' = 550 Pa, values comparable to those of the AMULIT material. Examining the 3D fluorescence images, we found that printed silicone features broke up and formed spherical droplets within the aqueous support. When a liquid ink is printed into a packed granular support medium, the smallest stable feature has a diameter given by $d_{min} \approx 2\gamma/\sigma_y$, where γ is the interfacial tension between the ink and the support medium (*15*). For the aqueous medium, γ = 25 mN/m, so d_{min} was ≈5 mm,

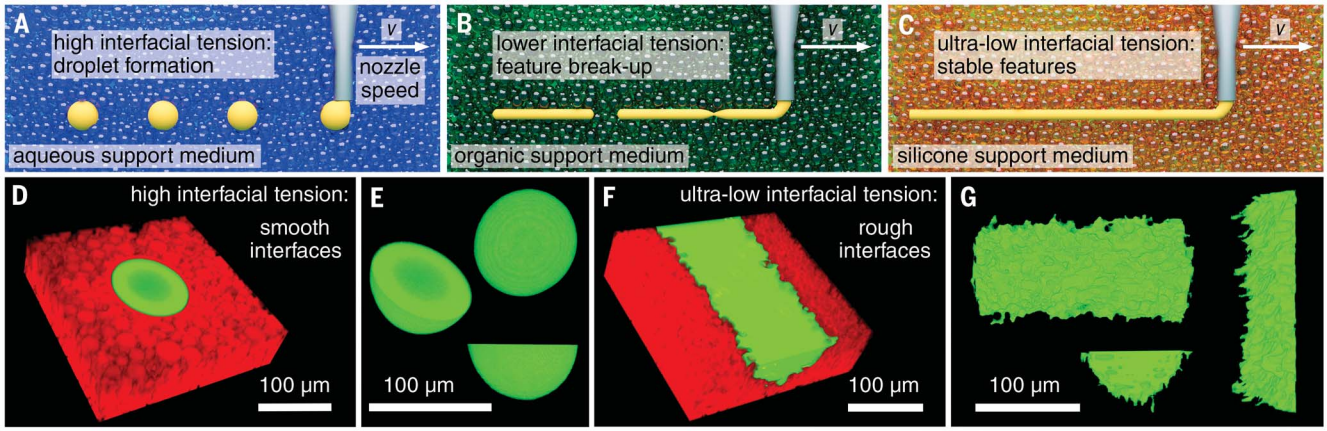

Fig. 1. Interfacial tension drives feature breakup in embedded 3D printing. (**A**) High interfacial tension between aqueous support materials and silicone inks destabilizes 3D printed features, driving them to break into spherical droplets. (**B**) Intermediate interfacial tension between organic support materials and silicone inks provides some stability but limits minimum stable feature size. (**C**) Ultralow interfacial tension between silicone oil–based support materials and silicone inks eliminates interfacial instabilities, removing the limits on minimum stable feature size. (**D**) CFM image showing silicone-based inks (green) that break into droplets when printed into support materials made from aqueous microgels (red). (**E**) A droplet digitally isolated from the support and examined from different angles. The droplet appears nearly spherical and exhibits a smooth surface. (**F**) By contrast, the silicone-based ink (green) remains continuous and retains its shape indefinitely after printing into a silicone-based support material (red). (**G**) When viewed from different angles, the printed features exhibit roughness with a characteristic length scale of the microparticles composing the support material, facilitated by ultralow interfacial tension.

50 times the 100-μm diameter of the printed feature (Fig. 1, D and E). Thus, the breakup of the feature into droplets was expected. By contrast, the 100-μm diameter silicone feature printed into the AMULIT support material remained intact, indicating that $\gamma < 0.5$ mN/m. To better estimate γ between a PDMS ink and the AMULIT support medium, we performed a series of test prints in which d_{min} was measured for multiple values of σ_y, finding that $\gamma \approx 0.08$ mN/m (fig. S4). We also observed that the characteristic roughness length scale at the feature surface was about one order of magnitude smaller than the feature diameter, from which we would estimate $\gamma \approx 0.05$ mN/m. These results indicate that the AMULIT approach can potentially achieve features 300 to 500 times smaller than those achievable when printing PDMS into an aqueous support medium having the same material properties.

Complex device fabrication using the AMULIT technique

The improvement in complexity, quality, and functionality of PDMS vessel models traced in the published literature parallels a decrease in interfacial tension of silicone inks against their embedding materials. For example, hydrocarbon support materials (*9*) improved on aqueous support materials (*19*). As a first test of the AMULIT method's capabilities, we printed a model brain aneurysm; models with accurate vasculature are needed for improved patient simulators to train neurosurgeons in cerebrovascular procedures. Current simulated tissues provide unrealistic tactile feedback, lack small-diameter intracranial angioarchitecture, and often exclude the aortic arch and extracranial vascular anatomy that determine which catheters and instruments are used in each procedure (*20*, *21*).

To create a model, we collected a 3D angiogram of a patient's brain aneurysm using x-ray computed tomography (XRCT). The 3D scan was segmented and processed to create a series of 3D printing trajectories (Fig. 2A and materials and methods). We used Gelest ExSil 100 silicone pre-elastomer, which can be formulated to have material properties that mimic a wide range of tissues. A snapshot from a video of the printing process demonstrates how the translating needle flows easily through the jammed emulsion, which traps the deposited silicone in place (Fig. 2B and movie S1). The printed structure was cured at 60°C for 24 hours and then imaged with XRCT (Fig. 2C). Horizontal and vertical slices through the 3D scan revealed that the highly branched, complex printed network of vessels is hollow, with an average wall thickness of ≈400 μm (Fig. 2D and movie S2). The CT scan of the printed structure was used to create a 3D model for quantitative comparison with the original angiogram. The registration between the patient-derived model and the printed model is excellent; 68% of the printed-surface locations lie within 500 μm of their programmed locations, and 95% lie within 1 mm (Fig. 2, E and F).

Our ability to accurately model brain vasculature raises the question of whether such fine structures can be manufactured to be both highly compliant and physically robust. The artificial aortic heart valve belongs to a class of devices with such requirements. Native aortic heart valves are subject to dynamic mechanical loads during the cardiac cycle (*22*). Prosthetic replacement is widely used to treat aortic valve failure, yet the predominantly used mechanical valves and allogeneic- or xenogeneic-tissue valve replacements often result in mechanical failure, hemolysis, blood coagulation, or structural degradation due to calcification. A potential alternative is an artificial silicone valve prosthesis; silicone is established in vascular applications because of its hemocompatibility and durability (*22*–*27*). The AMULIT 3D printing method can be used to replicate the intricate semilunar shape of the thin aortic leaflets in manufactured silicone valves. We designed a model heart valve based on physiologically representative dimensions of the different valve components (Fig. 2, G and H, and fig. S5) (*28*). We used a UV-curable silicone formulation, Silopren UV Electro-225-1 (Momentive), as the ink and printed it into the AMULIT material (Fig. 2I). To create highly flexible leaflets, we printed the structure by translating the needle tip at a speed of 2 mm/s and depositing material at a rate of 125 μL/hour, producing features ≈150 μm in diameter. Correspondingly, we chose a layer spacing of 100 μm for good layer adhesion. The printed model was then UV cured, removed from the AMULIT material, washed with detergent, and rinsed in deionized water (materials and methods). The cured part had a final wall thickness of ≈250 μm. Despite having very thin, flexible walls, the model valves were physically robust enough to connect to pipe

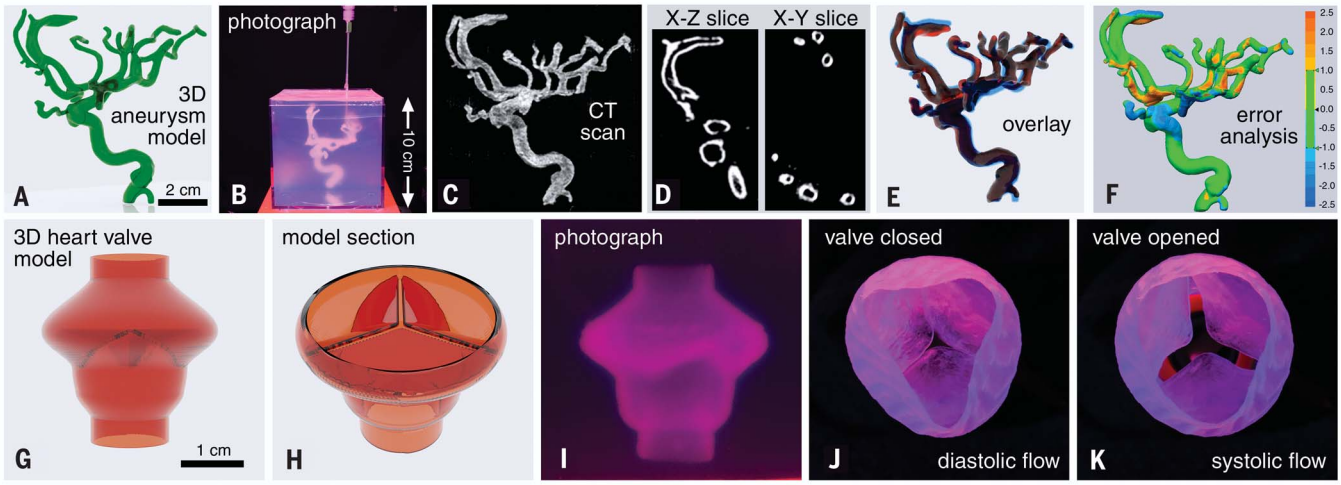

Fig. 2. AMULIT printing of brain aneurysm and aortic heart valve models. (**A**) Brain aneurysm models for surgical simulations comprise complex, interconnected, hollow tubes with intricate details. (**B**) Photograph of the aneurysm model being printed into the AMULIT material. (**C**) CT imaging of the 3D printed model within the printing container shows the complexity of the printed aneurysm. (**D**) Slices through the CT scan show that the printed structure exhibits the hollow channels of the patients' neurovasculature. (**E** and **F**) The printed structure overlays well with the patient's neurovasculature, and quantitative error analysis demonstrates agreement between the two (±1 mm error range corresponds to 95% of all points). (**G** and **H**) A model tricuspid aortic heart valve designed by using the geometric measurements of the native heart valve. (**I**) A silicone heart valve model printed in a single seamless trajectory with a wall thickness of 250 μm within the AMULIT support medium and cured under a UV lamp. (**J** and **K**) Once cured and washed, the valve model is robust enough to be coupled with a water supply, simulating transvalvular flow of the cardiac cycle. The thin leaflets of the valve are observed to open and close during the systolic and diastolic flow of the simulation.

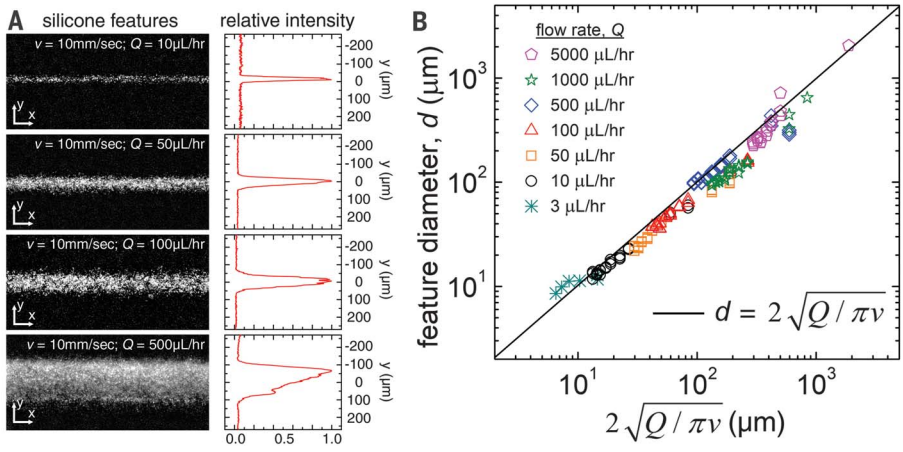

Fig. 3. Control of AMULIT printed feature size. (**A**) (Left) Intensity-inverted images. These images are averaged along the *x* axis, yielding an intensity profile across each feature. (Right) A Gaussian function is fit to the intensity profile to determine the diameter of the printed line. We measured printed feature diameter with brightfield microscopy, varying the translation speed, v, of the printing nozzle and the ink deposition rate, *Q*. (**B**) Feature diameter of the printed silicone is controllable and can be predicted from a fluid continuity equation with no fitting parameters.

fittings and simulate transvalvular blood flow through cyclic pumping of water (movie S3). During the negative flow of the pulse representing the diastolic cycle, the valves remained closed with very little deflection on the thin leaflets (Fig. 2J), and during the positive pulse corresponding to the systolic cycle, the leaflets deflected, opening the valve and letting the water flow (Fig. 2K).

AMULIT performance: Feature size and print quality

The wall thicknesses of the brain vasculature and heart valve models were set by using a combination of feature diameter and layer spacing. The feature diameter, *d*, for different prints, can be chosen by selecting a combination of nozzle translation speed, v, and material deposition rate, *Q*. To systematically explore how well *d* can be predicted with the AMULIT technique, we printed a series of linear features using the Smooth-On Mold Max 10 PDMS formulation at different combinations of v and *Q* and then measured *d* (Fig. 3A and materials and methods).We predicted the relationship between *d*, *Q*, and v, given by $\pi\,(d/2)^2 = Q/v$, according to basic fluid continuity. Performing many experiments at different combinations of *Q* and v, we found that this prediction matched the measured feature diameter very well with no adjustable parameters (Fig. 3B). These printed features were stable over time; the change in measured feature size over the course of 120 min postprinting was found to be negligible (fig. S6). We were able to fabricate stable silicone features as small as 8 μm in diameter using the AMULIT printing technique; the smallest stable feature diameter we have seen previously demonstrated with unmodified silicone was 40 μm, although smaller unstable features were also reported (*9*). A feature diameter of 10 μm was previously achieved by modifying silicone ink with emulsion droplets (*16*, *29*). To print these very fine features, we formulated an AMULIT support material with an increased yield stress using droplets 1 μm in diameter (fig. S1); the high-magnification images in Fig. 1F indicate that larger droplets would impose interfacial roughness comparable to these small feature diameters.

We have shown that highly controlled 3D printing with PDMS is possible with the AMULIT

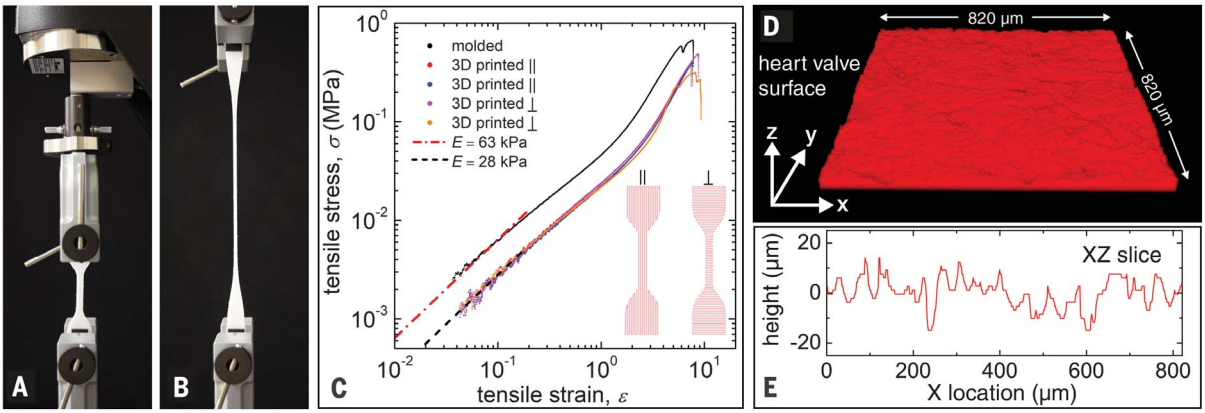

Fig. 4. Material and surface properties of the AMULIT printed silicone structures. (**A** and **B**) Silicone tensile specimens are subject to unidirectional tensile stress and are stretched to failure. (**C**) Tensile stress-strain curves of the specimens printed with their features oriented parallel and perpendicular to the tensile force show linear stress-strain relationships at low strains and exhibit an elastic modulus of 28 kPa. (**D** and **E**) Surface profiles of the printed silicone heart valves exhibit microroughness with an RMS value of 5.5 μm, likely determined by the emulsion droplet radius and the ultralow interfacial tension with the AMULIT support material.

technique, and the functionality of the heart valve model suggests that such structures may be sufficiently compliant and durable for use in applications. To test the mechanical performance of printed silicone structures, we fabricated tensile specimens using PlatSil-71 RTV (room-temperature vulcanizing) (Polytek) silicone formulation following ASTM standard D412 Type C specifications. To test the role of layer-to-layer adhesion in the mechanical integrity of the samples, we printed them with their extruded features oriented in both the longitudinal and lateral directions with respect to the long axis of the specimen geometry. The printed structures were cured at 60°C for 4 hours and then tested by using an Instron 5943 at a loading rate of 500 mm/min (Fig. 4, A and B). The tensile stress-strain data showed that both the lateral and longitudinal print specimens differed negligibly from one another and had the same elastic modulus of 28 kPa (Fig. 4C). All printed specimens exhibited linear stress-strain relationships at low strain levels and repeatable stress-strain curves at higher strains, failing at strains greater than 1000%. Comparing these results with the performance of molded specimens, we found that all the stress-strain curves had the same shape but that printed structures failed at higher strains than molded structures, whereas molded structures exhibited elastic moduli approximately twice those of printed structures. This softening effect could arise from systematic heterogeneities in the printed structures inherent to the 3D printing process. Additionally, we conducted fatigue tests, imposing 10^5 cycles of ±10% strain, alternately stretching and buckling the samples. Subsequent tensile tests showed that the printed structures exhibited less fatigue than did their molded counterparts; the elastic modulus dropped by 18% for the cast samples and 14% for the printed structures (fig. S7).

As a final assessment of the quality of structures fabricated with the AMULIT printing technique, we investigated the surface finish of fabricated parts. The ultralow interfacial tension between the silicone and the AMULIT support material was expected to produce microrough surfaces on the printed shapes. Using CFM, we imaged a segment of the heart valve model immersed in a rhodamine solution, visualizing and quantifying the surface roughness in 3D. We found the root mean square (RMS) roughness to be 6.54 ± 0.95 μm (mean and standard error, respectively) which is comparable to the average diameter of emulsion droplets used in these tests, ≈4 μm. Thus, we expect a smaller roughness with smaller emulsion droplets such as those used to print very fine features (Fig. 3B). This value is also comparable to the roughness of PDMS structures printed into support materials that exhibit a high interfacial tension against silicone inks (*9*), so it may be limited by other factors. In either case, our results demonstrate that eliminating disruptive interfacial driving forces with the AMULIT technique enables precise silicone printing without reducing surface quality or mechanical performance of fabricated structures. The added role of emulsion droplet size in surface roughness may enable a printed structure's optical properties to be tuned while independently controlling its mechanical performance through ink composition or feature diameter.

Conclusions

The AMULIT 3D printing method eliminates the disruptive effects of interfacial tension between printed inks and their support materials. Our results show that AMULIT printing can be used to make precise, smooth, strong, and functional devices from commercially available PDMS formulations. The versatility of the AMULIT technique eliminates the need to formulate specialized PDMS inks for 3D applications and broadens the toolbox for researchers and industrial manufacturers seeking to 3D print PDMS-based devices, while improving on previous silicone printing methods. The AMULIT strategy hinges on formulating support materials that are chemically similar to the inks they support—in this case, PDMS inks printed into a continuum of PDMS oil—although the same principle could be used with aqueous polymers. Despite the chemical similarity between the ink and the support medium, we never observed intermixing between the two materials that interfered with printing quality. The very low Reynolds number exhibited during embedded 3D printing with materials such as those we used should facilitate the formation of ink–support interfaces (*30*), potentially stabilized by an effective interfacial tension (*31*) or a form of liquid–liquid phase separation (*32*), likely influenced by the jammed emulsion phase. Additionally, weak attractive interactions between the emulsion droplets may help to retain them on their side of the interfaces (*33*–*35*). In the near term, we envision the AMULIT method to be useful in 3D printing for a wide range of applications beyond silicone-based devices, given the diversity and availability of polymer systems and the simplicity of formulating AMULIT support materials.

REFERENCES AND NOTES

1. H. H. Moretto, M. Schulze, G. Wagner, in *Ullmann's Encyclopedia of Industrial Chemistry* (Wiley VCH, 2011), pp. 23–26.
2. A. Rahimi, A. Mashak, *Plast. Rubber Compos.* **42**, 223–230 (2013).
3. X. Ruan *et al.*, *Adv. Mater. Technol.* **5**, 2000171 (2020).

4. A. Nathan *et al*., *Proc. IEEE* **100**, 1486–1517 (2012).
5. O. D. Yirmibeşoğlu *et al*., in *2018 IEEE International Conference on Soft Robotics* (*RoboSoft*), Livorno, Italy, 24 to 28 April 2018 (IEEE, 2018), pp. 295–302.
6. F. Liravi, E. Toyserkani, *Addit. Manuf.* **24**, 232–242 (2018).
7. V. Ozbolat *et al*., *ACS Biomater. Sci. Eng.* **4**, 682–693 (2018).
8. T. Femmer, A. J. Kuehne, M. Wessling, *Lab Chip* **14**, 2610–2613 (2014).
9. C. S. O'Bryan *et al*., *Sci. Adv.* **3**, e1602800 (2017).
10. T. Bhattacharjee *et al*., *Sci. Adv.* **1**, e1500655 (2015).
11. T. Bhattacharjee *et al*., *Soft Matter* **14**, 1559–1570 (2018).
12. G. Ovarlez, Q. Barral, P. Coussot, *Nat. Mater.* **9**, 115–119 (2010).
13. L. Mohan, C. Pellet, M. Cloitre, R. Bonnecaze, *J. Rheol.* (*N.Y.N.Y.*) **57**, 1023–1046 (2013).
14. J. R. Seth, L. Mohan, C. Locatelli-Champagne, M. Cloitre, R. T. Bonnecaze, *Nat. Mater.* **10**, 838–843 (2011).
15. C. S. O'Bryan, A. Brady-Miné, C. J. Tessmann, A. M. Spotz, T. E. Angelini, *Soft Matter* **17**, 3886–3894 (2021).
16. B. M. Rauzan, A. Z. Nelson, S. E. Lehman, R. H. Ewoldt, R. G. Nuzzo, *Adv. Funct. Mater.* **28**, 1707032 (2018).
17. C. Perrinet, E. J. Courtial, A. Colly, C. Marquette, R. Fulchiron, *Adv. Mater. Technol.* **5**, 1901080 (2020).
18. T. G. Mason, J. Bibette, D. A. Weitz, *Phys. Rev. Lett.* **75**, 2051–2054 (1995).
19. T. J. Hinton, A. Hudson, K. Pusch, A. Lee, A. W. Feinberg, *ACS Biomater. Sci. Eng.* **2**, 1781–1786 (2016).
20. M. Waqas *et al*., *Neurosurgery* **87**, E445–E453 (2020).
21. T. Scullen, J. D. Nerva, P. S. Amenta, A. S. Dumont, *Neurosurgery* **87**, E454–E455 (2020).
22. F. B. Coulter *et al*., *Matter* **1**, 266–279 (2019).
23. M. A. Punchard *et al*., *Ann. Biomed. Eng.* **37**, 1322–1330 (2009).
24. R. N. Ghriallais, L. McNamara, M. Bruzzi, *J. R. Soc. Interface* **10**, 20120965 (2013).
25. L. Rouleau, J. Rossi, R. L. Leask, *J. Biomech. Eng.* **132**, 071015 (2010).
26. J. Martorell *et al*., *Cardiovasc. Res.* **103**, 37–46 (2014).
27. M. Balcells *et al*., *Circulation* **121**, 2192–2199 (2010).
28. W. Sun, C. Martin, T. Pham, *Annu. Rev. Biomed. Eng.* **16**, 53–76 (2014).
29. Z.-T. Xie, D.-H. Kang, M. Matsusaki, *Soft Matter* **17**, 8769–8785 (2021).
30. K. J. LeBlanc *et al*., *ACS Biomater. Sci. Eng.* **2**, 1796–1799 (2016).
31. D. Truzzolillo, L. Cipelletti, *Soft Matter* **13**, 13–21 (2016).
32. S. Duraivel *et al*., *Biophys. Rev.* **3**, 031307 (2022).
33. V. V. Erramreddy, S. Ghosh, *Langmuir* **30**, 11062–11074 (2014).
34. A. Z. Nelson, R. H. Ewoldt, *Soft Matter* **13**, 7578–7594 (2017).
35. A. Z. Nelson *et al*., *Curr. Opin. Solid State Mater. Sci.* **23**, 100758 (2019).
36. S. Duraivel, T. E. Angelini, Heart Valve Maker, v2.0, Zenodo (2023); https://doi.org/10.5281/zenodo.7643835.

ACKNOWLEDGMENTS

The authors thank Anton Paar for use of their MCR 702 rheometer through the Anton Paar VIP research program. **Funding:** No funding was received. **Author contributions:** Conceptualization: S.D. and T.E.A. Methodology: S.D., D.L., D.A.R., G.M.S., A.M.S., B.S.S., S.A.B., F.J.B., and T.E.A. Investigation: S.D., D.L., D.A.R., A.M.S., and T.E.A. Visualization: S.D., D.L., D.A.R., A.M.S., B.S.S., S.A.B., F.J.B., and T.E.A. Funding acquisition: B.S.S., S.A.B., F.J.B., and T.E.A. Project administration: T.E.A. Supervision: B.S.S., F.J.B., and T.E.A. Writing – original draft: S.D. and T.E.A. Writing – review and editing: S.D., D.L., D.A.R., G.M.S., A.M.S., B.S.S., S.A.B., F.J.B., and T.E.A. **Competing interests:** S.D., B.S.S., and T.E.A are inventors on a US patent application (PCT/US2021/037346). All other authors declare that they have no competing interests. **Data and materials availability:** All data are available in the manuscript and the supplementary material; code for the design and generation of print trajectories for the heart valve model is freely accessible at Zenodo (*36*).

SUPPLEMENTARY MATERIALS

science.org/doi/10.1126/science.ade4441
Materials and Methods
Supplementary Text
Figs. S1 to S7
Movies S1 to S3

Submitted 17 August 2022; accepted 17 February 2023
10.1126/science.ade4441